Robotics & Computer-Integrated Manufacturing, Vol. 8, No. 2, pp. 103–111, 1991
Printed in Great Britain

0736-5845/91 $3.00 + 0.00

● *Paper*

TRANSIENT LATERAL MOTION OF ROBOTS IN PART MATING

Y. YAO

Department of Mechanical Engineering, University of Wollongong, P.O. Box 1144, Wollongong, N.S.W. 2500, Australia

This paper is concerned with achieving a higher rate at which a robot operation involving part mating can be carried out while free of excessive contact forces. It is shown that the rate is primarily limited by the robot end effector's lateral transient response to the contact forces, while the response depends mainly on the link inertia characteristics and joint compliances. Both factors were modelled and simulated for robots of SCARA configuration for the chamfer-crossing stage. The transient response predicted by the model led to determination of a varying-speed insertion motion for the chamfer-crossing stage to avoid large initial impacts between peg and hole and to limit the contact force during the entire stage. The discrepancy angle between the contact force and the resultant lateral motion was also considered. Good agreement was obtained between the transient response predicted in simulation and that observed in experiment.

I. INTRODUCTION

An important requirement for obtaining higher productivity rates in robot operations involving mating of rigid parts is that the insertion motions be free of excessive contact forces. If all parts were perfectly made and positioned, mating could always be carried out at the maximum speed of the robot and free of excessive mating forces. However, practical constraints such as cost and technical limitations cause parts to differ, and robots and jigs to wear; consequently, parts are misplaced and misaligned at the moment of mating.

Instead of resorting to expensive methods such as eliminating errors in advance or sensing and correcting errors during operations, research has been reported on robot compliance which accommodates these misplacements and misalignments during mating. Studies on the intrinsic compliance of a robot have been reported[1,3,4] where a relationship between joint compliance and compliance at the end effector of a robot was derived under the assumption of rigid links. The relationship enables one to estimate whether the intrinsic compliance of a robot is sufficient to achieve a successful mating operation for a given robot repeatability and mating tolerance. If not, additional compliance may be added to a robot, such as a remote compliance center (RCC) device.[2] The effectiveness of a given RCC depends on the part geometry and stiffness, and is usually best suited for a limited range of part sizes.

In studies of both intrinsic and externally added compliances in mating, an assumption was that the mating is carried out at a relatively low speed. Therefore, static methods were used to derive the equilibrium conditions for a successful mating.[8] If, however, one is interested in achieving the highest possible cycle rate of a mating process, dynamic effects have to be considered.

This paper addresses the dynamic effects during the chamfer crossing stage for SCARA robot operations involving part mating. Figure 1 shows that, to avoid excessive contact forces, the insertion motion $\Delta z(t)$ has to be determined according to the lateral response $\Delta r(t)$ under the action of the contact force $N(t)$. First,

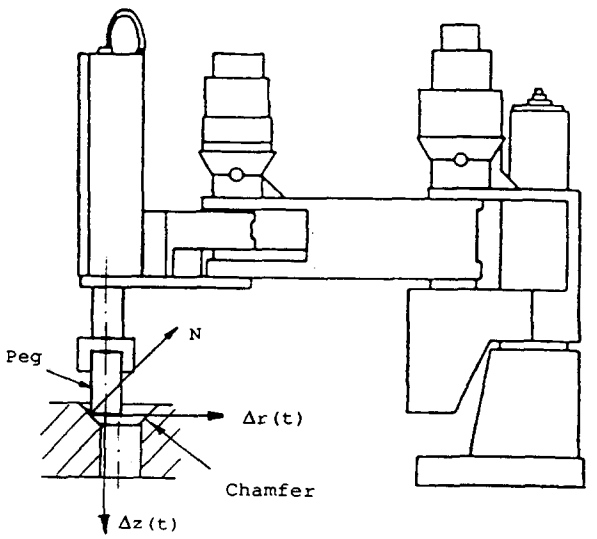

Fig. 1. Lateral response Δr and insertion motion Δz.

the geometric compatibility condition of a chamfer-crossing motion free of excessive contact force was derived. Then, an algorithm to predict the lateral response $\Delta r(t)$ of the robot end effector was obtained by modeling robot dynamics where rigid links and torsional spring joints were assumed. On that basis, a varying-speed insertion motion $\Delta z(t)$ was formulated. The entire procedure was validated and compared in both simulation and experiment. Close correlation between the response predicted by the simulation and that observed in experimental data was obtained. Implementation of the varying-speed insertion motion achieved mating free of overshoot.

II. GEOMETRICAL COMPATIBILITY OF CHAMFER CROSSING MOTION FREE OF EXCESSIVE CONTACT FORCES

Parts under consideration were assumed to be rigid and have a cylindrical geometry. Joints 1, 2, and 3 of a SCARA robot shown in Fig. 2 articulate on parallel vertical axes and the workpiece is inserted vertically; hence the robot primarily provides compliance on the horizontal plane and the compliance is mainly attributed to joint rotational compliance.[6] Therefore, only the lateral component of a contact force is considered.

Figure 3a shows a typical cylindrical part mating during the chamfer-crossing stage. Because of the misplacements and misalignments discussed above, the peg always contacts the chamfer first. The resultant contact force is denoted as $N(t)$ and the lateral component is $N_l(t)$. The net lateral force can be shown as

$$\begin{aligned} F_l(t) &= N_l(t) - \mu N(t)\cos\alpha \\ &= N(t)\sin\alpha - \mu N(t)\cos\alpha \end{aligned} \tag{1}$$

where μ is the friction coefficient of the mating surfaces and α is the chamfer angle. The force $F_l(t)$ causes the end effector's lateral response which eventually leads the peg into the hole. To avoid excessive contact forces during chamfer-crossing, the insertion motion $\Delta z(t)$ has to be determined according to the lateral response, $\Delta r(t)$. If the peg is inserted too fast, the chamfer will be pressed too hard and the contact force will momentarily rise to a fairly large value which may result in part damage.

Such a relation between $\Delta r(t)$ and $\Delta z(t)$ can be established by resolving $\Delta r(t)$ into two perpendicular components, a lateral $\Delta r_l(t)$ and tangential $\Delta r_t(t)$. The displacement, $\Delta r_l(t)$, produces a downward $\Delta z_l(t)$ given by

$$\Delta z_l(t) = \Delta r_l(t)\tan\alpha \tag{2}$$

Note that $\Delta r_t(t)$ causes an upward $\Delta z_t(t)$ as shown in Fig. 4a and given by

$$\Delta z_t(t) = ((R^2(t) + \Delta r_t^2(t))^{1/2} - R(t))\tan\alpha \tag{3}$$

where $R(t)$ is the instantaneous radius from the contact point to the center of the hole. Thus, the total insertion displacement as a function of lateral responses is

$$\begin{aligned} \Delta z(t) &= \Delta z_l(t) - \Delta z_t(t) \\ &= (\Delta r_l(t) - ((R^2(t) + \Delta r_t^2(t))^{1/2} - R(t))\tan\alpha. \end{aligned} \tag{4}$$

Equation 4 relates the lateral motion $\Delta r(t)$ to the insertion motion $\Delta z(t)$ and describes the geometrical compatibility condition for chamfer crossing motion free of contact forces. For implementation, $\Delta z(t)$ in Eq. (4) can be determined as follows.

- Specify allowable contact forces $F_x(t)$ and $F_y(t)$ shown in Fig. 4b and obtain lateral responses

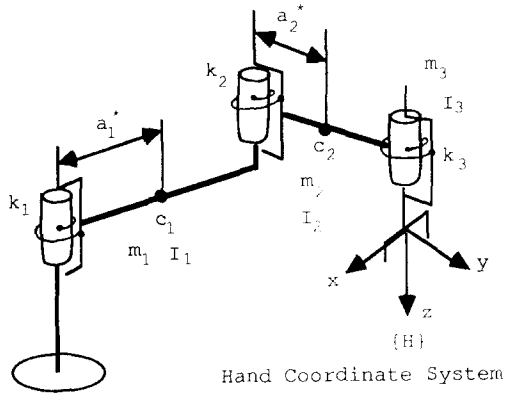

Fig. 2. Simplified dynamic and joint stiffness model of a SCARA robot.

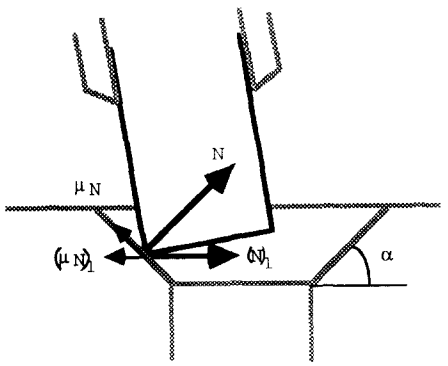

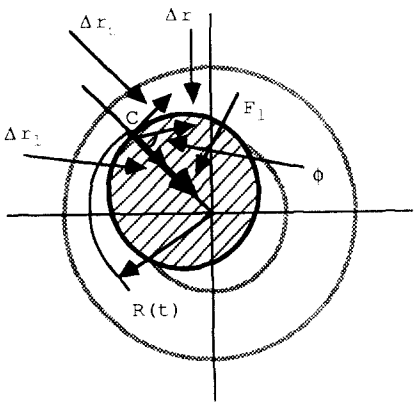

Fig. 3. Schematic of peg-chamfer contact. (a) Chamfer-crossing (side view). (b) Chamfer-crossing (top view).

$\Delta x(t)$ and $\Delta y(t)$ via solving dynamic equations outlined in next section first.

- Calculate

$$\Delta r(t) = (\Delta x^2(t) + \Delta y^2(t))^{1/2} \tag{5}$$

$$\psi(t) = \tan^{-1}(F_y(t)/F_x(t))$$

and

$$\phi(t) = \tan^{-1}(\Delta y(t)/\Delta x(t)) - \psi(t) \tag{6}$$

where $\psi(t)$ is the angle between the lateral force $F_l(t)$ and x axis in $\{H\}$, and $\phi(t)$ is the angle between $F_l(t)$ and resultant lateral motion $\Delta r(t)$ shown in Fig. 3b.

- Calculate

$$\Delta r_l(t) = \Delta r(t)\cos\phi(t)$$

and

$$\Delta r_t(t) = \Delta r\,(t)\sin\phi(t). \tag{7}$$

- Finally, let $R(t) = R$, which is the nominal radius of the mating parts, and substitute $\Delta r_l(t)$, $\Delta r_t(t)$ and R into Eq. (4) to obtain $\Delta z(t)$. Its derivatives are determined by numerical methods.

III. MODELING ROBOT DYNAMICS DURING CHAMFER CROSSING

To model robot inertial and other dynamic effects during chamfer-crossing, the following assumptions were made. Since the SCARA robot shown in Fig. 2 primarily provides a degree of compliance in the horizontal plane, only three rotational joints were modeled. With the SCARA design, the robot arm members are normally quite massive and can be regarded as rigid links. The bearings are also assumed to be rigid[6] because the joints have larger deflections in comparison.

For a mating process by a SCARA robot, a peg is usually carried to a location above the hole by the rotational joints 1, 2, and 3 of the robot, then insertion in the z-direction is activated. Therefore joints 1, 2, and 3 are held stationary by their motors during insertion, and joint rotational deflections are due to joint stiffness only. Suppose the joint angles before contacting the chamfer are $\boldsymbol{\theta}_0 = (\theta_{10}\ \theta_{20}\ \theta_{30})^T$ and the joint stiffness is $\mathbf{k} = (k_1\ k_2\ k_3)^T$ as shown in Fig. 4. Then the vector dynamics in joint space is

$$\mathbf{M}(\boldsymbol{\theta})\ddot{\boldsymbol{\theta}} + \mathbf{V}(\boldsymbol{\theta}, \dot{\boldsymbol{\theta}}) + \mathbf{K}(\boldsymbol{\theta}, \boldsymbol{\theta}_0) = \boldsymbol{\tau} \tag{8}$$

where $\boldsymbol{\theta} = (\theta_1\ \theta_2\ \theta_3)^T$ are joint variables, $\boldsymbol{\tau}$ is a 3×1 vector of joint torques, $\mathbf{M}(\boldsymbol{\theta})$ is a 3×3 symmetric inertia matrix, and $\mathbf{V}$ is a 3×1 vector of centrifugal and Coriolis terms. The difference between Eq. (8) and conventional dynamics formulations is in the third term

$$\mathbf{K}(\boldsymbol{\theta}, \boldsymbol{\theta}_0) = (k_1(\theta_1 - \theta_{10})\ k_2(\theta_2 - \theta_{20})\ k_3(\theta_3 - \theta_{30}))^T \tag{9}$$

which is a 3×1 vector of joint stiffness terms. The gravitational term is not included because the three links remain at the same level all the time.

For a given robot, Eq. (8) can be formulated and a simulation carried out as follows. The allowable contact forces $F_x(t)$ and $F_y(t)$ are specified in the hand coordinate system $\{H\}$ and corresponding joint torques are calculated by[5,8]

$$\boldsymbol{\tau}(t) = \boldsymbol{\tau}_a(t) + \mathbf{J}_H^T(t)(F_x(t), F_y(t), 0)^T \tag{10}$$

where $\mathbf{J}_H(t)$ is the 3×3 Jacobian matrix written in $\{H\}$ and $\boldsymbol{\tau}_a(t)$ represents a vector of torques generated by joint actuators. The torque term in $\{H\}$ was taken as zero assuming cylindrical part mating. A numerical method can be used to solve differential equations in Eq. (8) for given values of $\boldsymbol{\tau}(t)$ and the results are then converted back to $\{H\}$ by

$$(\Delta x(t), \Delta y(t), 0) = \mathbf{J}_H(t)\Delta\boldsymbol{\theta}(t)$$

and

$$(\Delta \dot{x}(t), \Delta \dot{y}(t), 0) = \mathbf{J}_H(t)\Delta\dot{\boldsymbol{\theta}} \tag{11}$$

where t emphasizes the time-varying nature of the Jacobian matrix; but the simulation results presented in next section shows that $\mathbf{J}_H(t)$ is almost constant for small changes of joint angles.

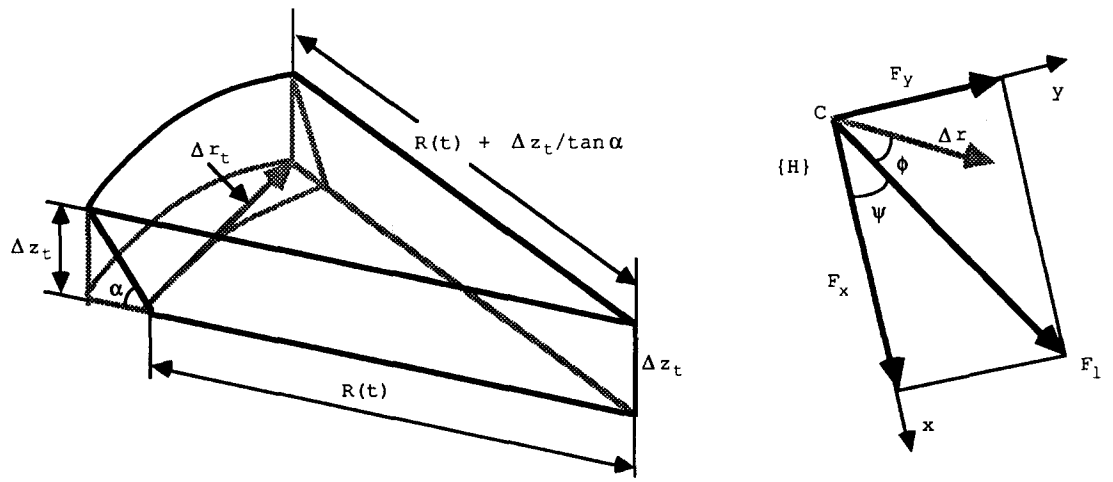

Fig. 4. Relationship between $\Delta r(t)$ and $\Delta z(t)$ [Eq. (4)]. (a) Schematic for Eq. (4). (b) Schematic for Eqs. (5) to (7).

IV. SIMULATION

An IBM 7545 SCARA robot was used for simulation and experiment. First, step contact force inputs $F_x(t)$ and $F_y(t)$ of various step sizes were assumed. Figure 5a shows one of the step inputs where $F_x = F_y = 25$ N. The inputs were transformed to the joint space via Eq. (10). Figure 5b and c shows torques τ_1 and τ_2 at joints 1 and 2, respectively. Both τ_1 and τ_2 were almost constant because the configuration change during chamfer-crossing is so small that $\mathbf{J}_H(t)$ in Eq. (10) is almost constant. Joint angles θ_1 and θ_2 shown in Fig. 6a and b as well as their derivatives shown in Fig. 6c and d were obtained by solving the coupled nonlinear differential equations in Eq. (8), using an IMSL subroutine IVPAG which is based on the Adam Moulton method. Figure 7 shows the end effector's responses, $\Delta x(t)$ and $\Delta y(t)$, as well as their derivatives using Eq. (11). Figure 8a and b shows the total responses and total velocity in the hand coordinate system $\{H\}$ calculated by

$$\Delta r(t) = \sqrt{\Delta x^2 + \Delta y^2} \text{ and } \Delta \dot{r}(t) = \sqrt{\Delta \dot{x}^2 + \Delta \dot{y}^2}. \quad (12)$$

As expected, the response $\Delta r(t)$ deviated from the force vector $F = (F_x^2(t) + F_y^2(t))^{1/2}$ by an angle $\phi \approx 30°$ depicted in Fig. 8c, because the configuration does not provide a true compliance center. The effect of the deviation angle ϕ cannot be ignored and is considered below.

V. A VARYING-SPEED INSERTION MOTION

In the simulation example above, $F_x = F_y = 25$ N was assumed; that is, a constant contact force $F = (F_x^2(t) + F_y^2(t))^{1/2} = (25^2 + 25^2)^{1/2} = 35.36$ N and a constant angle $\psi = \tan^{-1}(F_y(t)/F_x(t)) = 45°$ were assumed. In reality, however, the angle ψ is unpredictable, because a peg could contact a chamfer at any point C shown in Fig. 3b. Therefore, the angle ψ could be any value between 0° to 360°. Shown in Fig. 9a and b are total response and velocity of the end effector resulting from a step input $F = 35.36$ N with different possible values of ψ. It is seen that when ψ is near 0° or 180°, the robot has the slowest response. Figure 9c further reveals that the deviation angle ϕ between the force and the resultant response is also a function of ψ. The largest ϕ occurs when ψ is close to 22.5° or 157.5°. In order to determine which value corresponds to the worst case, $\Delta r(t)$ was converted to $\Delta z(t)$ via Eqs. (2) to (4) for $\psi = 0°$, 22.5°, 157.5° and 180° illustrated in Fig. 10a. It became clear that although the angle ψ cannot be predicted, the synthesis will always be on the safe side if it is based on the worst case where ψ is near 0° or 180°. In a real assembly operation, ψ may be not close to 0° or 180° at all but the contact force will always be less than or at most equal to the allowed value. Figure 10c and d is the synthesis results of z motion during a cross-chamfer stage which guarantees a contact force not greater than 35.36 N. Figure 10d indicates that the best strategy to mating a peg in

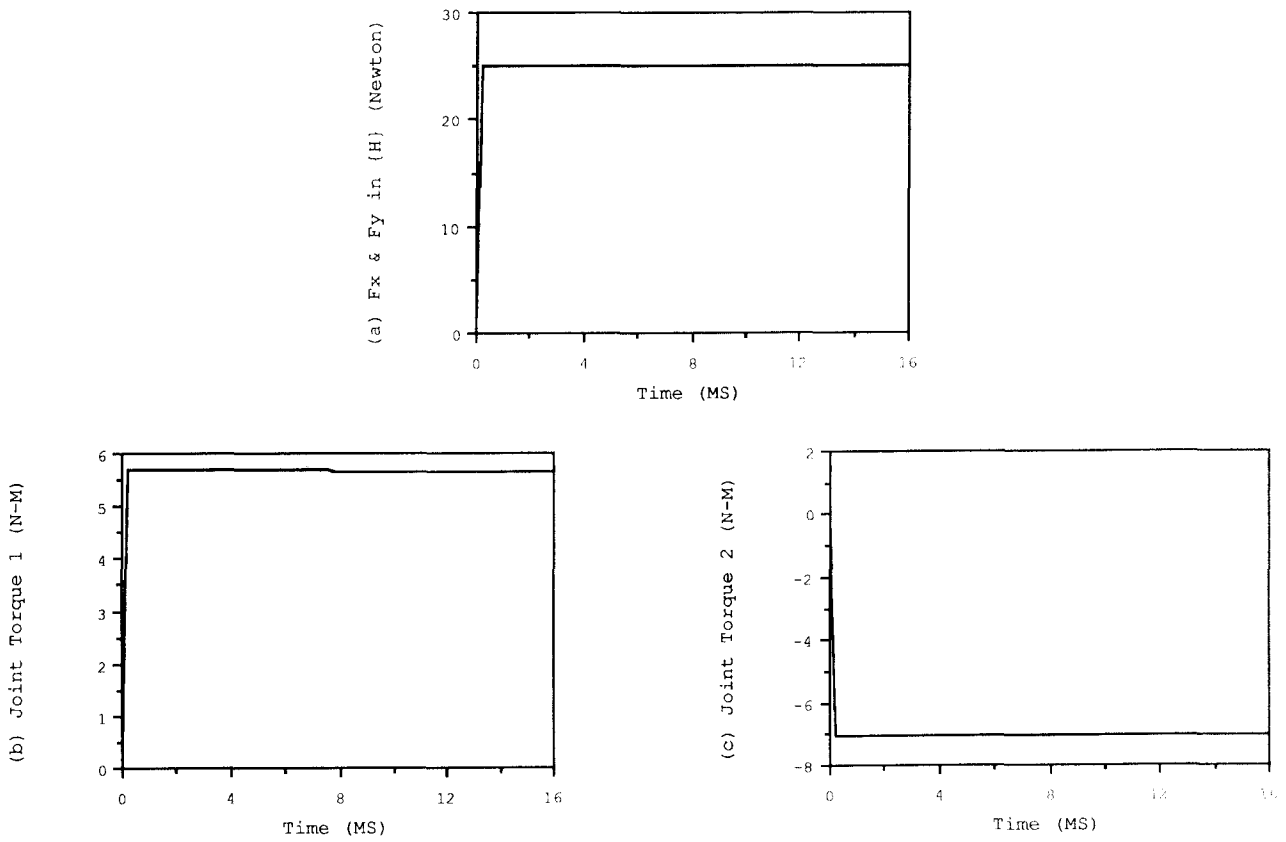

Fig. 5. Contact forces in $\{H\}$ and corresponding joint moments.

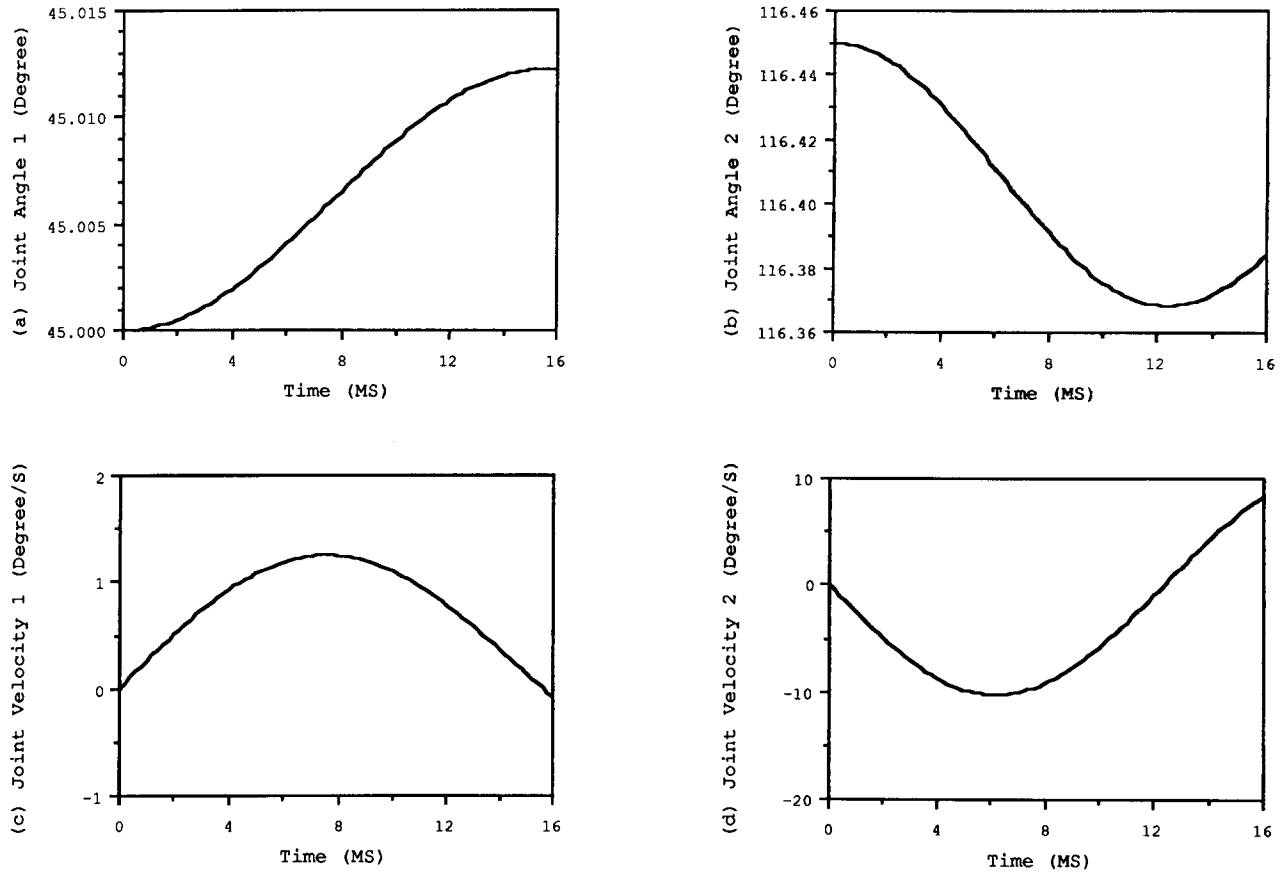

Fig. 6. Joint angular deflections and their rates.

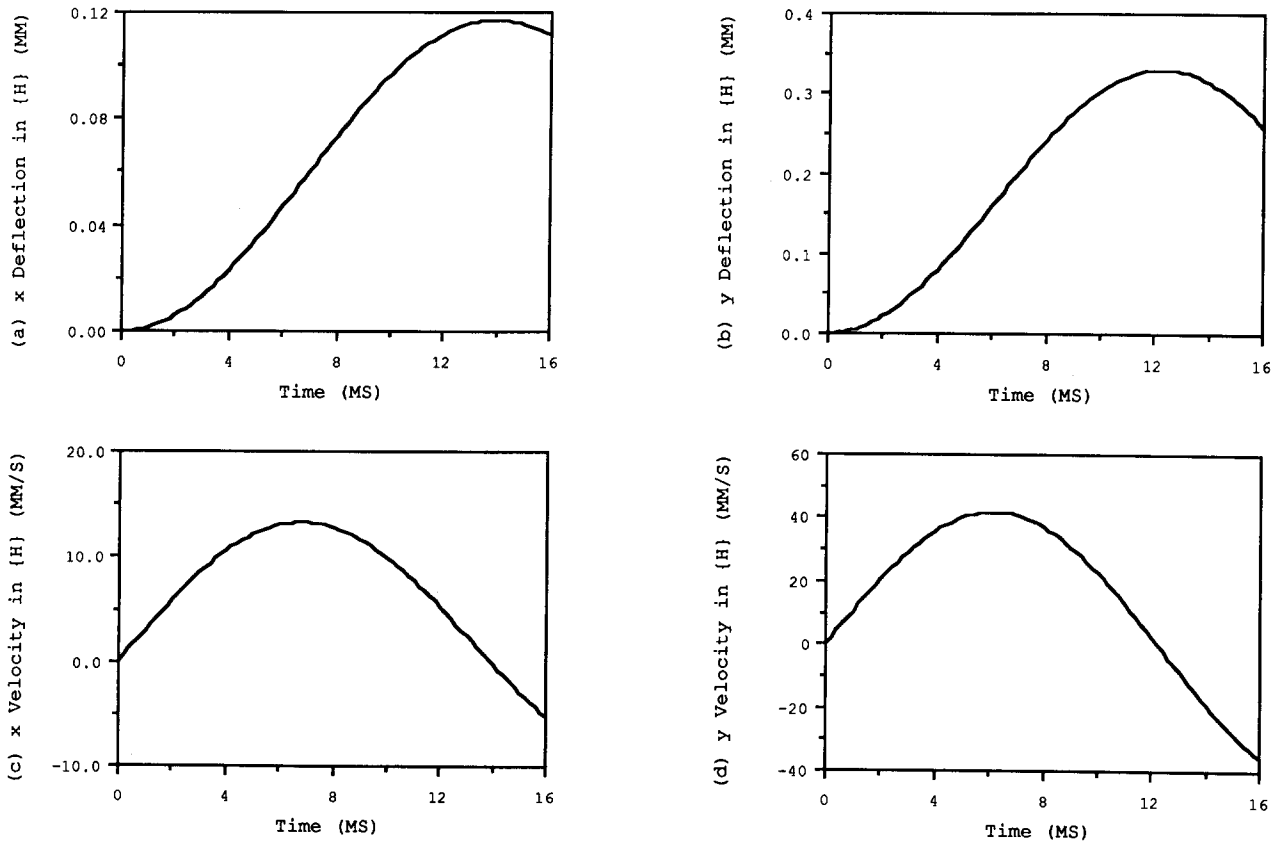

Fig. 7. End effector x and y deflections and their rates, all in $\{H\}$.

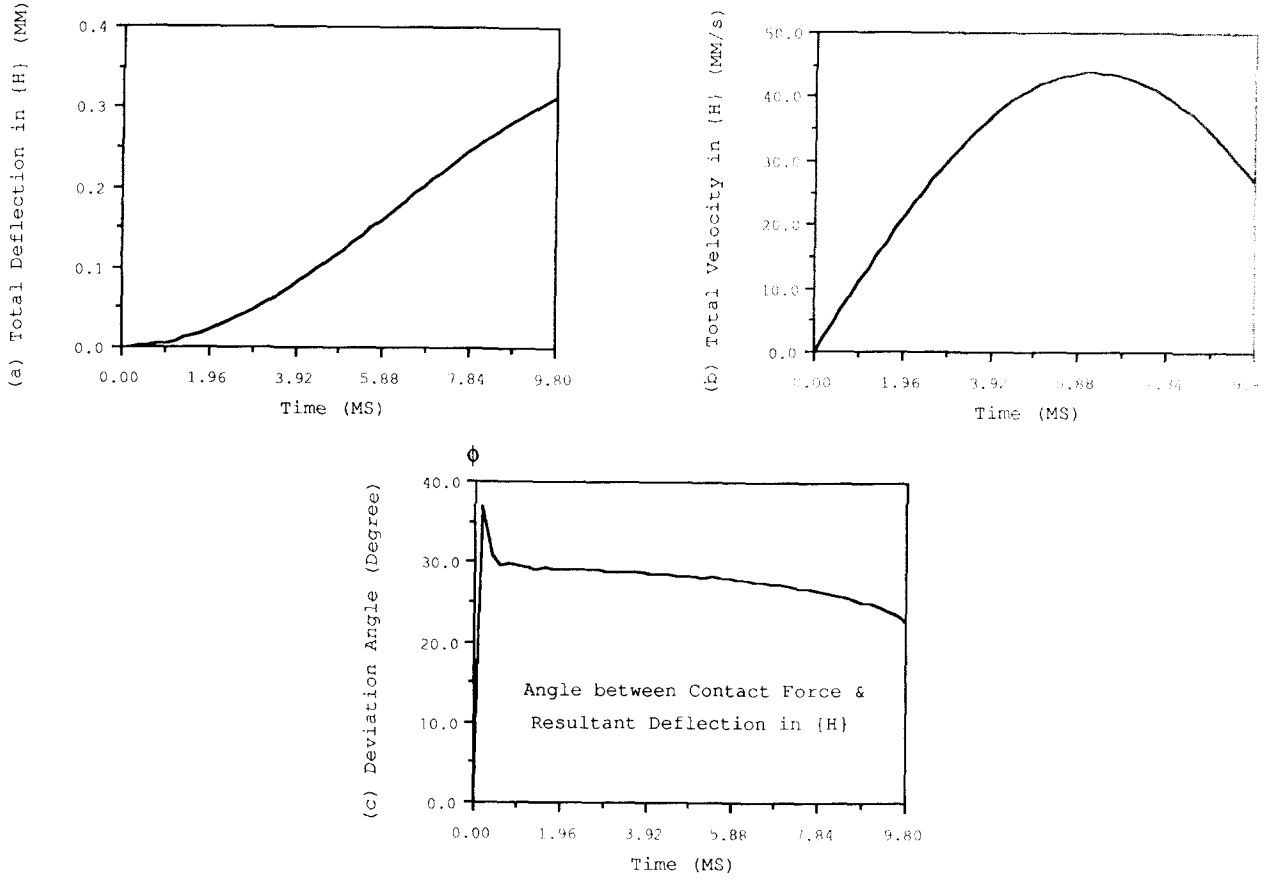

Fig. 8. Total end effector deflection, its rate and deviation angle ϕ, all in $\{H\}$.

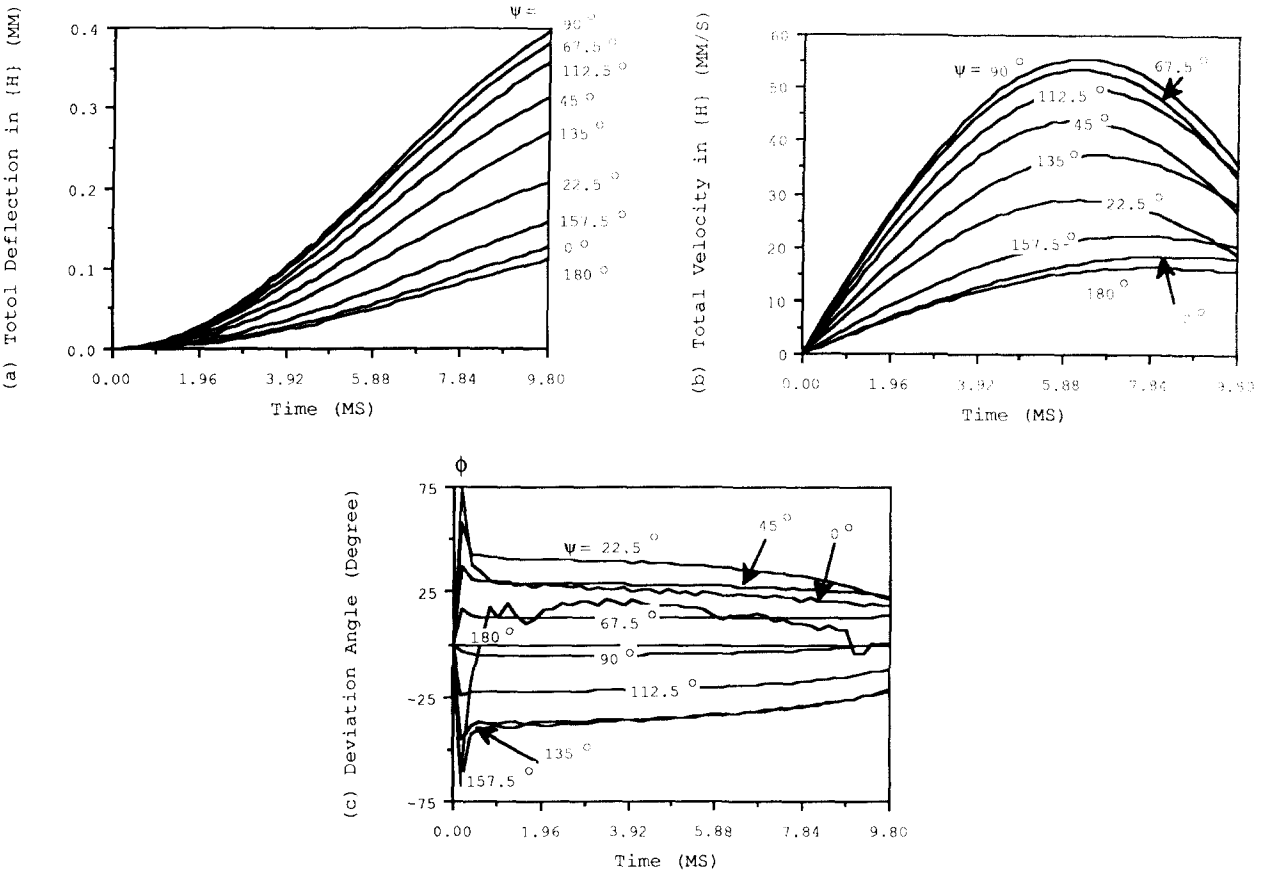

Fig. 9. Comparison of total deflections, their rates and deviation angle ϕ for different ψ.

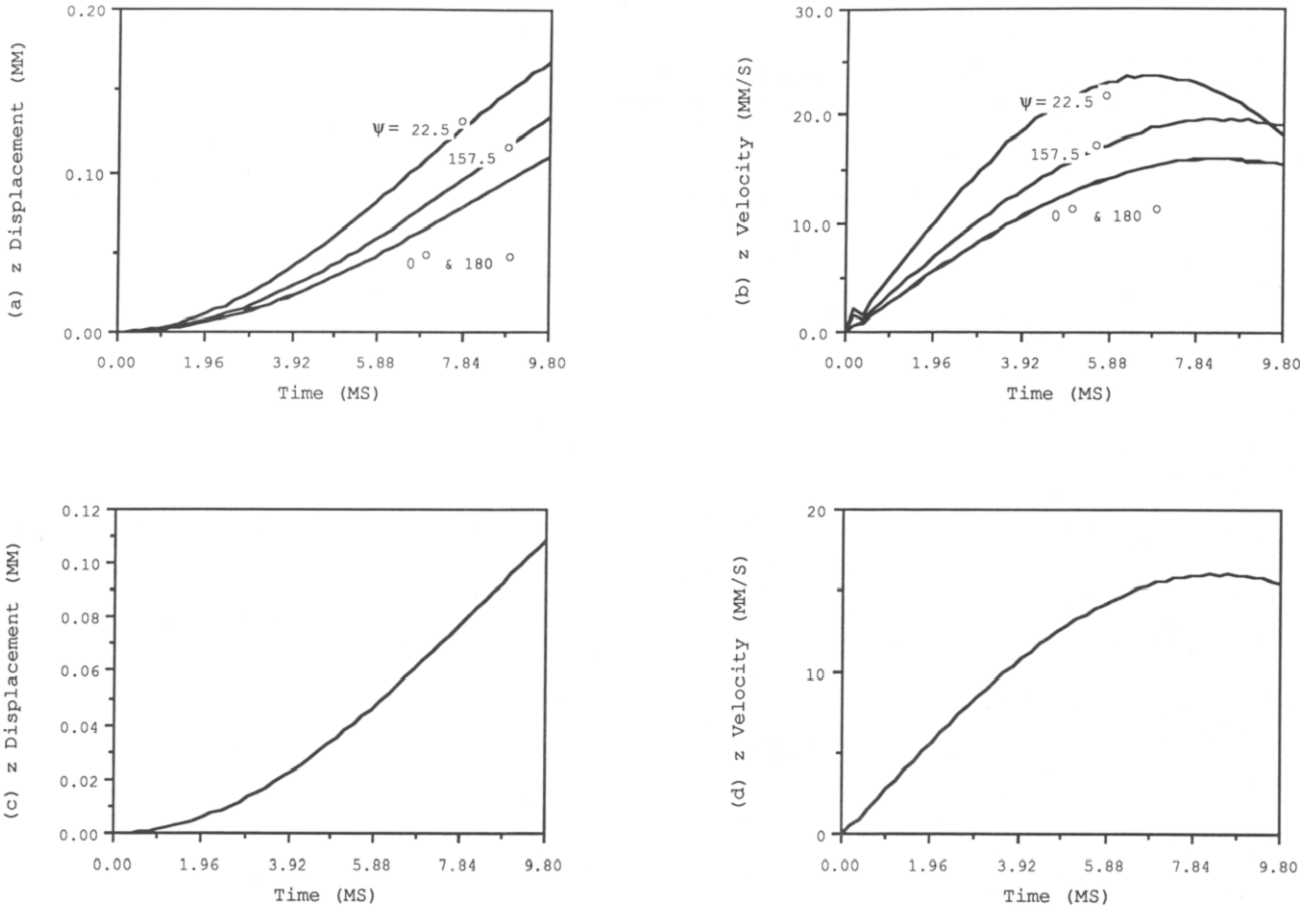

Fig. 10. Comparison among worst cases and synthesis example.

a hole at the highest possible rate without excessive contact forces is the following: approach the hole at full speed, stop before the peg touches the chamfer, and restart the z-axis following the varying-speed insertion motion formulated in this paper.

VI. EXPERIMENTAL RESULTS AND DISCUSSION

The purpose of the experiments was to validate the simulated prediction of lateral response, $\Delta r(t)$, and to implement the varying-speed insertion motion.

The simulation results were validated using the apparatus shown in Fig. 11. A set of four strain gauges mounted on a simulated peg recorded the forces applied in both x and y directions in $\{H\}$, while two eddy current probes recorded the resultant lateral responses in corresponding directions. A typical record of the contact forces was plotted in Fig. 12a and b and the resultant responses were recorded in Fig. 12c and d. The contact forces shown in Fig. 12a and b were digitized and used as inputs to the simulation program. The lateral responses are overlaid on Fig. 12c and d for comparison. Good agreement between the response predicted by the simulation and the actual response was obtained. This indicates that the approximations made for the dynamic modeling are reasonable. Thus the dynamic simulation of the contact process provides a valid prediction of the lateral response of the end effector; in turn, the varying-speed insertion motions based on the prediction is valid.

An experiment involving the mating of a peg in a hole, shown in Fig. 13, was conducted. Figure 14a and b shows actual contact forces recorded at a mating experiment using the proposed varying-speed cross-chamfer motion and the conventional constant-speed motion, respectively. Apparently, the varying-speed motion avoided the initial impacts.

Since most robots have relatively low joint flexibility, the increment of joint angles under the action of

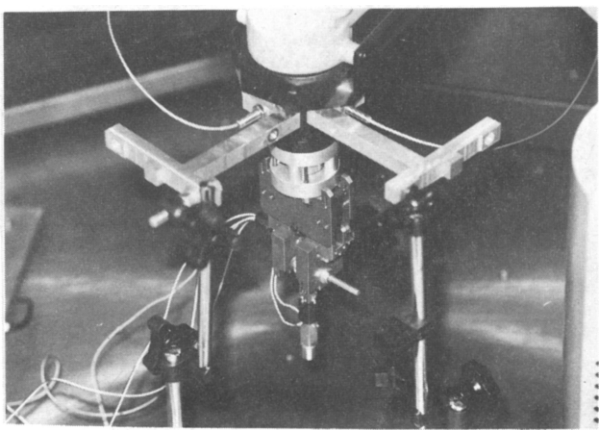

Fig. 11. Dynamic modeling validation apparatus.

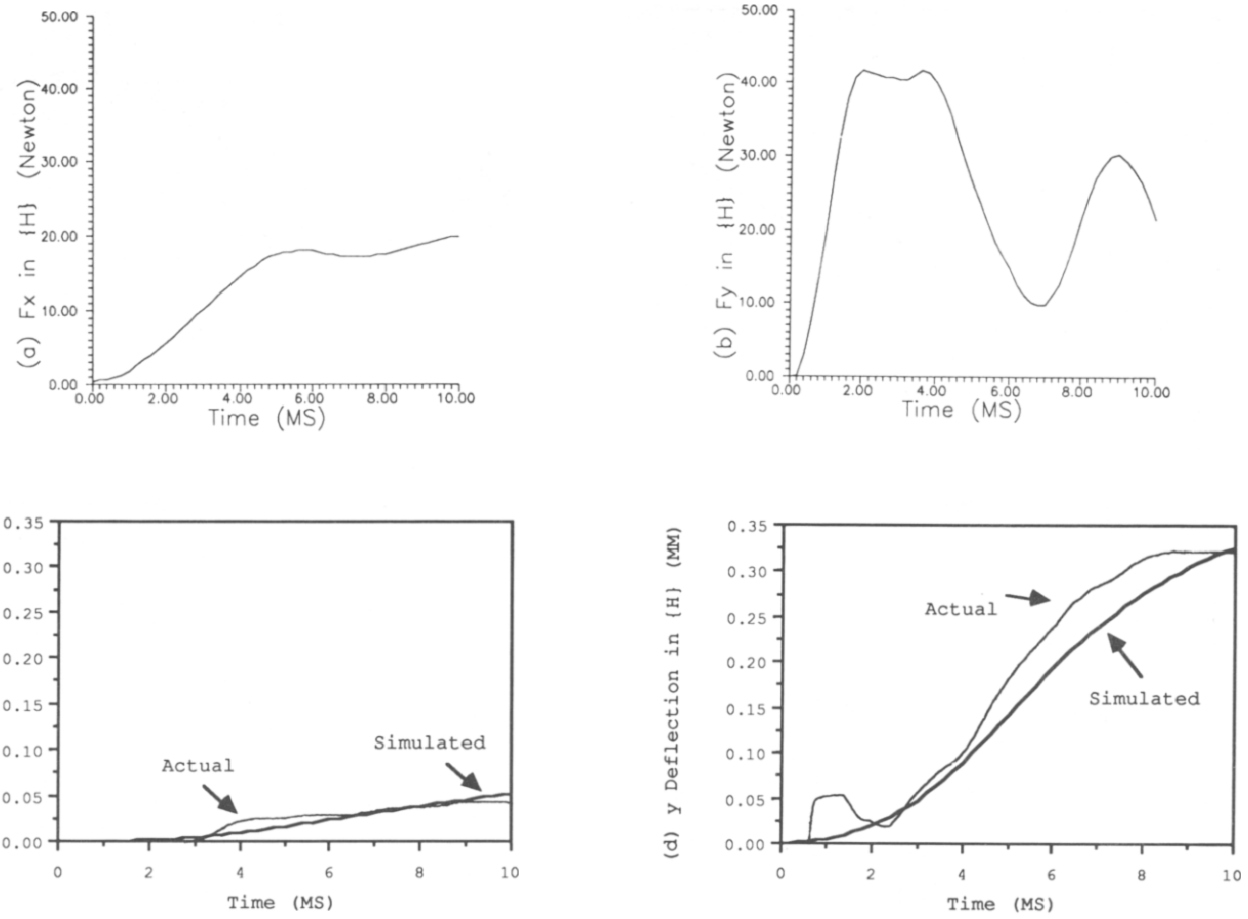

Fig. 12. Comparison of simulated and actual deflections.

the contact forces at the end effector is normally very small, so that the system nonlinearity is negligible [see Eq. (11)]. Otherwise the proposed strategy may become less effective. In order to synthesize a varying-speed insertion motion for a given robot, its system parameters have to be known accurately.

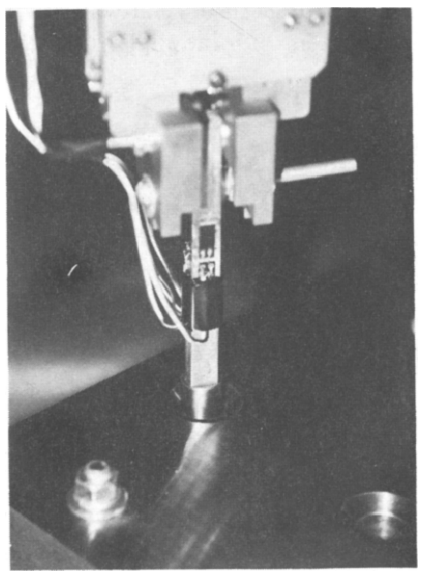

Fig. 13. Peg-hole mating experiment.

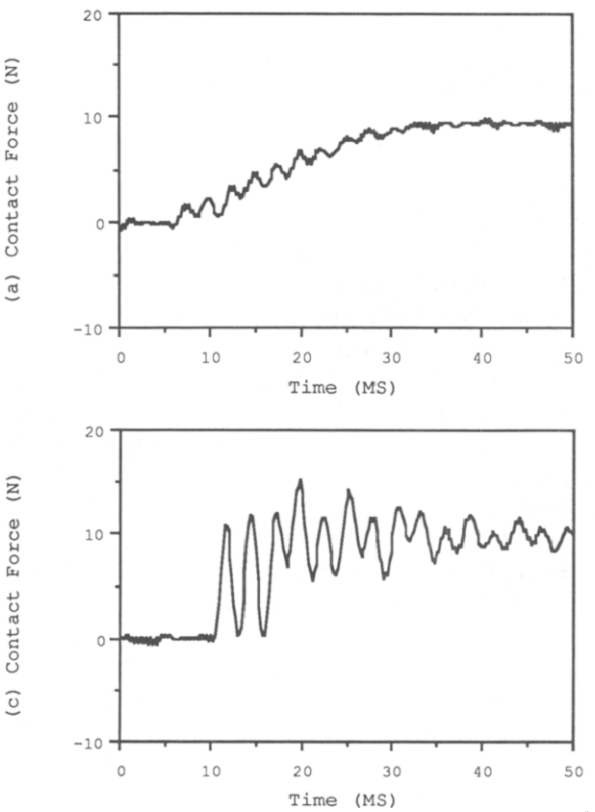

Fig. 14. Experimental contact forces during the chamfer-crossing stage. (a) Using the varying-speed insertion motion (b) Using the constant-speed insertion motion.

VII. CONCLUSIONS

The end effector's lateral response to contact forces was predicted in simulation and validated by experiment. On that basis, a varying-speed insertion motion was formulated to avoid excessive contact forces while the robot is being used to its maximum capability. The conventional method, using a constant speed in both the approaching and the chamfer-crossing stages, is constrained to use a lower speed to avoid excessive contact forces in the latter stage. In contrast, the varying-speed insertion motion allows the use of the highest possible speed in the approaching stage and a varying speed determined by the end effector lateral deflection rate in the chamfer-crossing stage.

REFERENCES

1. Bourrieres, J. P., Jeannier, P., Lhote, F.: Intrinsic compliance of position-controlled robots—applications in assembly. Proc. 5th International Conference on Assembly Automation, Paris, France, 22-24 May 1984, pp. 133-142.
2. Drake, S. H., Spencer, R. H., Simunovic, S. N.: Using compliance in assembly—an engineering approach to float. SME Technical Paper MS79-873, 1979.
3. Elmaraghy, H. A., Johns, B.: An investigation into the compliance of SCARA robots. Part I: Analytical model. *ASME Trans. J. Dynamic Systems Measurement Control* **110**: 18-22, March 1988.
4. Elmaraghy, H. A., Johns, B.: An investigation into the compliance of SCARA robots. Part II: Experimental and numerical validation. *ASME Trans. J. Dynamic Systems Measurement Control* **110**: 23-30, March 1988.
5. Kankaanranta, R. K., Koivo, H. N.: Dynamics and simulation of compliant motion of a manipulator. *IEEE J. Robotics Automation* **4**(2): 163-173, April 1988.
6. Leu, M., Dukovski, V., Wang, K. K.: Effect of mechanical compliance on deflection of robot manipulators. *Ann. CIRP* **36**: 305-309, 1987.
7. Paul, R. P.: *Robot Manipulators: Mathematics, Programming and Control.* MIT Press, 1981.
8. Whitney, D. E.: Quasi-static assembly of compliantly supported rigid parts. *ASME Trans. J. Dynamic Systems Measurement Control* **104**: 65-77, March 1982.